*Journal of Sound and Vibration* (1999) **227**(3), 479–510
*Article No.* jsvi.1999.2387, available online at http://www.idealibrary.com on IDEAL®

# THE ROLE OF MOMENTS ON THE VIBRATION TRANSMISSION IN BUILT-UP STRUCTURES

R. A. FULFORD† AND B. A. T. PETERSSON

*AAETS, Loughborough University, Loughborough LE*11 3*TU, England*
†*Institut für Technische Akustik, Technische Universtät Berlin*, 10587 *Berlin, Germany*

(*Received* 10 *November* 1998, *and in final form* 5 *March* 1999)

Towards the development of simplified analysis methods for the vibrational power in built-up plate structures, a circular can upon an infinite recipient plate is considered. The primary aspect considered is the role of the moments at the upper and lower interfaces, with respect to both the input and transmitted power. Where the thickness of the cans top-plate is at least twice that of the side-wall, the moments are shown to have limited influence and, within "engineering accuracy", it is suggested they can be ignored in an analysis. This greatly simplifies the modelling of the system. Moreover, it is also shown that where the side-walls are thick compared to the top-plate and, accordingly, the rotational stiffness at the upper interface high, the influence of the moments can, and most simply, be accounted for by merely imposing a guided boundary condition upon the top-plate. A substantial simplification results for the modelling of the system and the analysis. Further, it is found that for typical dimensions, there is an extended frequency range over which the response of the side-walls is either mass or stiffness controlled. Thence, it follows that the input and transfer mobilities of the side-walls are comparable to each other, leading to further reduction of the models.



## 1. INTRODUCTION

For a complete analysis of vibration transmission in built-up plate structures, all wave motion transmitted across all boundaries has to be taken into account. Since this transmission process often involves both translational and rotational components and several boundaries, the analysis is frequently multi-dimensional and the demands for a solution inevitably high. Problems relating to the vibration transmission in built-up place structures are therefore usually approached using numerical techniques such as finite element analysis. Although these techniques are purported to be a method of analysis, the inherent drawback is that the physical behaviour of the system is not revealed. Any forthcoming solution is therefore

†Present address: Institut für Technische Akustik, Technische Universtät Berlin, 105787 Berlin, Germany.

0022-460X/99/430479 + 32 $30.00/0 

directly relevant only to the particular structure studied and cannot be immediately extended to aid the analysis of another. With respect to design this necessitates therefore many repeated calculations. As a tool, numerical methods can therefore be both laborious and capricious in use.

A more defined approach is to attempt an analytical formulation. Commonly this is achieved by first sub-dividing the system into those elementary structural components for which expressions for the structural characteristic (i.e., mobility or impedance) can be obtained, and then recombining via continuity and force equilibrium these elementary components to reform the whole structure [1]. Whilst if all degrees of freedom are accounted for, at all boundaries, the approach does not lead away from a multi-dimensional analysis, the inherent advantage is that it does lead to an understanding of the physical behaviour of the system. With this insight it is often possible to determine a dominant behaviour. Identification of a dominant behaviour permits the multi-dimensional analysis to be reduced and, if the reductions are significant, a simplified model is procured. This reduced model can then be used as the basis for an engineering design tool.

With such an approach in mind, the notionally simple, built-up structure of a transversally force excited box upon an infinite recipient plate is considered. It is noted that herein a distinction is made between box-like and column-like superstructures whence the height of the box is less than its cross-sectional dimensions whereas the opposite is assumed for a column. This only implies, however, that the lateral motion in the former case is essentially governed by shear or the global interface bending of the recipient. The primary hypothesis addressed is then that the power transmitted is dominated by that associated with the transverse force ($F$), at both the upper and lower interfaces of the side-walls, such that the moment induced power at these interfaces ($M$) can be neglected for a wide, practically important frequency range.

## 2. BOX UPON INFINITE PLATE

Focusing on the efficacy of moment and force transmission, it is argued that a can (circular-like box) can be substituted for a rectangular-like box. In contrast to a rectangular-like box, no vertical side-wall discontinuities are present in the circular case. Although this will ensure a different set of eigenfrequencies it is argued that with respect to the hypothesis this will not obscure the salient physics of the system. This is so because the relative contributions of moment and force can be expected to be primarily determined by the boundary conditions at the upper and lower interfaces of the side-walls. Moreover, since the details of a structures dynamic response are known to be sensitive to all involved parameters, i.e., material, dimensions, boundary conditions and excitation, it can be argued that where all the details are not known, i.e., at the design stage, a theoretical model merely has to "capture" the main trends of the response that are relevant and that this is, therefore, all that needs to be modelled. Accepting such reasoning, the introduction of a circular can as opposed to a rectangular-like box is then motivated in that it simplifies the mathematical treatment. Firstly, it reduces the

system such that only three structural elements are involved; a circular top-plate, a cylindrical side-wall and an infinite recipient plate, see Figure 1. Secondly, for each of these "circular" elements, the line mobility concept can be invoked via a Fourier series expansion in the spatial domain [2], which facilitates the re-assembling of the three sub-structures.

For a spatial dependence of form $\cos(n\theta)$ and including both moment and force, the complex power integrated around a circular interface is given by

$$Q = \pi[vF + wM]. \tag{1}$$

A list of symbols is given in Appendix C.

With reference to Figure 1 and assuming that there is no cross-coupling (translational to rotational) between the upper and lower interfaces of the side-walls, application of continuity gives the power at the input position and the upper and lower boundaries as

$$Q_{input} = \pi[Y_{Fv}^{00}F_0 + Y_{Fv}^{10}F_1 + Y_{Mv}^{10}M_1]F_0^*, \tag{2}$$

$$Q_{upper} = \pi[(Y_{Fv}^{22}F_2 + Y_{Fv}^{32}F_3)F_2^* + (Y_{Mw}^{22}M_2 + Y_{Mw}^{32}M_3)M_2^*]. \tag{3}$$

$$Q_{lower} = \pi[(Y_{Fv}^{33}F_3 + Y_{Fv}^{23}F_2)F_3^* + (Y_{Mw}^{33}M_3 + Y_{Mw}^{23}M_2)M_3^*] \tag{4}$$

respectively.

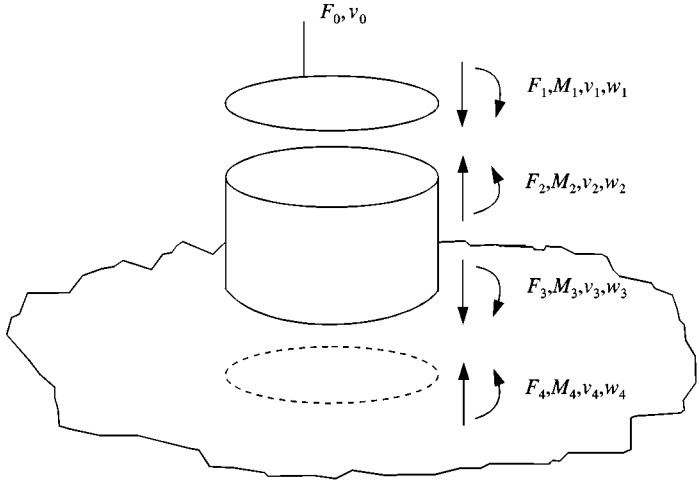


Figure 1. The three structural components of the circular can on a recipient system.

Via the application of a force balance, the forces and moments at the cylinder ends are obtained from

$$\begin{bmatrix} (Y_{Fv}^{22} + Y_{Fv}^{11}) & Y_{Fv}^{32} & Y_{Mv}^{11} & 0 \\ Y_{Fv}^{23} & (Y_{Fv}^{33} + Y_{Fv}^{44}) & 0 & Y_{Mv}^{44} \\ Y_{Fw}^{11} & 0 & (Y_{Mw}^{22} + Y_{Mw}^{11}) & Y_{Mw}^{32} \\ 0 & Y_{Fw}^{44} & Y_{Mw}^{23} & (Y_{Mw}^{33} + Y_{Mw}^{44}) \end{bmatrix} \begin{bmatrix} F_2 \\ F_3 \\ M_2 \\ M_3 \end{bmatrix} = \begin{bmatrix} Y_{Fv}^{01} F^0 \\ 0 \\ Y_{Fw}^{01} F_0 \\ 0 \end{bmatrix}. \tag{5}$$

To assess the influence of the moment and thereby test the hypothesis, calculations for the complete model can be compared with those from a reduced model in which all moment contributions are neglected.

For the reduced model the respective powers are

$$Q_{input} = \pi[Y_{Fv}^{00} F_0 + Y_{Fv}^{10} F_1] F_0^*, \tag{6}$$

$$Q_{upper} = \pi[Y_{Fv}^{22} F_2 + Y_{Fv}^{32} F_3] F_2^*, \tag{7}$$

$$Q_{lower} = \pi[Y_{Fv}^{33} F_3 + Y_{Fv}^{23} F_2] F_3^*, \tag{8}$$

with the forces obtained from

$$\begin{bmatrix} (Y_{Fv}^{22} + Y_{Fv}^{11}) & Y_{Fv}^{23} \\ Y_{Fv}^{23} & (Y_{Fv}^{33} + Y_{Fv}^{44}) \end{bmatrix} \begin{bmatrix} F_2 \\ F_3 \end{bmatrix} = \begin{bmatrix} Y_{Fv}^{01} F_0 \\ 0 \end{bmatrix}. \tag{9}$$

For the reduced model, only a limited amount of mobility data is therefore needed. Moreover, since only those mobilities which remain, $Y_{Fv}^{00}$, $Y_{Fv}^{01}$, $Y_{Fv}^{11}$, $Y_{Fv}^{22}$, $Y_{Fv}^{23}$ and $Y_{Fv}^{44}$, can be considered to represent the "bones" of the system it is difficult to conceive of an approach other than a lumped system analysis through which the data set can be reduced further, cf. reference [3].

## 3. MOBILITIES

### 3.1. TOP PLATE

Employing Love's theory of elasticity [4] and simple harmonic motion, the mobilities of the top-plate can be obtained following the modal formulation of Soedel [5].

With a free boundary condition imposed, i.e., $M_r = 0$ and $F_r = 0$ and computer-based search routines implemented to find the eigenfrequencies, the line mobilities relating force and moment to velocity become

$$Y_{Fv}^{00,01,11} = \sum_{m=0}^{\infty} \sum_{m=1}^{\infty} \frac{\mathrm{i}\omega\pi}{\rho h N_{mn}} \frac{\begin{pmatrix} \mathrm{J}_n(\lambda_{mn} r_0) + \\ (B_2/B_1)\mathrm{I}_n(\lambda_{mn} r_0) \end{pmatrix} \begin{pmatrix} \mathrm{J}_n(\lambda_{mn} r) + \\ (B_2/B_1)\mathrm{I}_n(\lambda_{mn} r) \end{pmatrix}}{(\omega_{mn}^2 - \omega^2 + \mathrm{i}\eta\omega_{mn}^2)} \cos(n\theta), \tag{10}$$

and,

$$Y_{Mv}^{01,11} = \sum_{n=0}^{\infty}\sum_{m=1}^{\infty} \frac{\mathrm{i}\omega\pi}{\rho h N_{mn}} \frac{\begin{pmatrix} (n/r_0)\mathrm{J}_n(\lambda_{mn}r_0) - \\ \lambda_{mn}\mathrm{J}_{n+1}(\lambda_{mn}r_0) + \\ (B_2/B_1)(n/r_0)\,\mathrm{I}_n(\lambda_{mn}r_0) + \\ (B_2/B_1)\lambda_{mn}\mathrm{I}_{n+1}(\lambda_{mn}r_0) \end{pmatrix} \begin{pmatrix} \mathrm{J}_n(\lambda_{mn}r) + \\ (B_2/B_1)\mathrm{I}_n(\lambda_{mn}r) \end{pmatrix}}{(\omega_{mn}^2 - \omega^2 + \mathrm{i}\eta\omega_{mn}^2)} \cos(n\theta), \tag{11}$$

for all mode orders except those relating to rigid-body motion. Descriptions for the various terms can be found in Appendix A.

For the "piston-like" translational rigid-body mode (0, 0) the mobilities are

$$Y_{Fv}^{00} = Y_{Fv}^{01} = Y_{Fv}^{11} = \frac{1}{\mathrm{i}\omega\rho h\pi a^2}, \tag{12}$$

whilst for the rotational rigid-body mode (0, 1),

$$Y_{Fv}^{00} = \frac{2r_0^2}{\mathrm{i}\omega\rho h\pi a^4}, \tag{13}$$

$$Y_{Fv}^{01} = \frac{2r_0}{\mathrm{i}\omega\rho h\pi a^3}, \tag{14}$$

$$Y_{Fv}^{11} = \frac{2r_0}{\mathrm{i}\omega\rho h\pi a^2}. \tag{15}$$

Differentiating equations (10) and (11) with respect to $r$ gives the mobilities relating force and moment to rotational velocity as

$$Y_{Fw}^{01,11} = \sum_{n=0}^{\infty}\sum_{m=1}^{\infty} \frac{\mathrm{i}\omega\pi}{\rho h N_{mn}} \frac{\begin{pmatrix} (n/r)\mathrm{J}_n(\lambda_{mn}r) - \\ \lambda_{mn}\mathrm{J}_{n+1}(\lambda_{mn}r) + \\ (B_2/B_1)(n/r)\,\mathrm{I}_n(\lambda_{mn}r) + \\ (B_2/B_1)\lambda_{mn}\mathrm{I}_{n+1}(\lambda_{mn}r) \end{pmatrix} \begin{pmatrix} \mathrm{J}_n(\lambda_{mn}r_0) + \\ (B_2/B_1)\mathrm{I}_n(\lambda_{mn}r_0) \end{pmatrix}}{(\omega_{mn}^2 - \omega^2 + \mathrm{i}\eta\omega_{mn}^2)} \cos(n\theta), \tag{16}$$

and

$$Y_{Mv}^{11} = \sum_{n=0}^{\infty} \sum_{m=1}^{\infty} \frac{\mathrm{i}\omega\pi}{\rho h N_{mn}} \times \frac{\begin{pmatrix} (n/r_0)\mathrm{J}_n(\lambda_{mn} r_0) - \\ \lambda_{mn}\mathrm{J}_{n+1}(\lambda_{mn} r_0) + \\ (B_2/B_1)(n/r_0)\,\mathrm{I}_n(\lambda_{mn} r_0) + \\ (B_2/B_1)\lambda_{mn}\mathrm{I}_{n+1}(\lambda_{mn} r_0) \end{pmatrix} \begin{pmatrix} (n/r)\mathrm{J}_n(\lambda_{mn} r) - \\ \lambda_{mn}\mathrm{J}_{n+1}(\lambda_{mn} r) + \\ (B_2/B_1)(n/r)\,\mathrm{I}_n(\lambda_{mn} r) + \\ (B_2/B_1)\lambda_{mn}\mathrm{I}_{n+1}(\lambda_{mn} r) \end{pmatrix}}{(\omega_{mn}^2 - \omega^2 + \mathrm{i}\eta\omega_{mn}^2)} \cos(n\theta). \tag{17}$$

These are valid for all $(m, n)$ other than the rotational rigid-body mode for which

$$Y_{Fw}^{01} = \frac{2r_0}{\mathrm{i}\omega\rho h\pi a^4}, \tag{18}$$

$$Y_{Fw}^{11} = \frac{2}{\mathrm{i}\omega\rho h\pi a^3}, \tag{19}$$

$$Y_{Mw}^{11} = \frac{2}{\mathrm{i}\omega\rho h\pi a^4}. \tag{20}$$

For $n = 0$, a mass-controlled region resulting from equation (12) is obtained prior to a resonant region. The fundamental resonance is at $k_{Biop}a = \pi/2$ and subsequent resonances are located at $m\pi/2$. An anti-resonance separates the mass- and resonant-controlled regions. In the resonant-controlled region the trend is, as expected, towards the characteristic plate mobility.

Where $n = 1$, a mass-controlled region followed by an anti-resonance and then a resonant region with trend of the characteristic plate mobility is found. For all other orders of $n$ an associated rigid-body mode, however, does not exist such that the behaviour prior to the resonant region is stiffness controlled, excluding a fundamental anti-resonance.

The format of the transfer mobility $Y_{Fv}^{01}$ (from the input force position to the translational response position at the edge of the plate) can be expected to be similar to that of $Y_{Fv}^{00}$ whereby for both $n = 0$ and 1 a mass-controlled region will be followed by a resonant-controlled region whilst for $n > 1$, a stiffness-controlled region will precede the resonant region. For $n = 0$ and 1 an anti-resonance will, however, not separate the mass- and resonant-controlled regions.

Clearly, when the response vector is rotational, i.e., for $Y_{Fw}^{01}$, $Y_{Fw}^{11}$ and $Y_{Mw}^{11}$, a mass-controlled region can only be expected for $n = 1$. For both $Y_{Fw}^{01}$ and $Y_{Fw}^{11}$, the rotational response will also mean that in the resonant region the characteristic trend will exhibit an order of magnitude increase per decade. For $Y_{Mw}^{11}$, the addition of a rotational excitation vector means a characteristic trend of two orders of magnitude increase per decade can be expected.

### 3.2. CYLINDRICAL SIDE-WALL

For an unprejudiced solution of the can dynamics, the mobilities should be developed for a cylinder that is free at its edges with respect to all of radial, axial and tangential motion. Such a solution is, however, difficult to obtain due to the inherent coupling between all three-degrees of freedom at the boundary. To permit some simplification, and in view of the distinction between box- and column-like superstructures, it is suggested that the completely free condition can be modified to one which is free with respect to both tangential and axial motion but simply supported with respect to radial motion, see Figure 2(a). Compared with the completely free condition the simply supported condition does impose a restriction upon the deformation of the cylinder, see Figure 2(b). Provided the cylinders' response is small and it is either translational (axial) or rotational (lateral), the deformation ($\delta$) will negligible. For the can, this is argued to be the case provided any resultant lateral force negligible. In cases where the "sway" will become significant, obviously, the boundary conditions of the cylinder would need to be modified or a shear beam model introduced.

Assuming therefore simple supports, Loves theory can be employed such that, as for the developments for the top plate, the work of Soedel can be followed whereby the mobility relating axial velocity to axial force is obtained as

$$Y_{Fv}^{22,23} = \sum_{i=1}^{3} \sum_{m=1}^{\infty} \frac{2i\omega(A_i/C_i)^2 \cos(m\pi x/L)\cos(m\pi x_0/L)}{\rho hL[(A_i/C_i)^2 + (B_i/C_i)^2 + 1][\omega_{imn}^2 - \omega^2 + i\eta\omega_{imn}^2]}, \tag{21}$$

whereas the mobility relating tangential rotational velocity to moment is developed as

$$Y_{Mv}^{22,23} = \sum_{i=1}^{3} \sum_{m=1}^{\infty} \frac{i\omega(2\pi^2)(m^2)\cos(m\pi x/L)\cos(m\pi x_0/L)}{\rho hL^3[(A_i/C_i)^2 + (B_i/C_i)^2 + 1][\omega_{imn}^2 - \omega^2 + i\eta\omega_{imn}^2]}. \tag{22}$$

Descriptions for the various terms can be found in Appendix B.

That the cylinder is free of constraint in the axial direction implies that a rigid-body mode must be included for the $n = 0$ component of $Y_{Fv}^{22,23}$,

$$Y_{Fv}^{22,23} = \frac{1}{i\omega\rho L\pi h(2a - h)}. \tag{23}$$

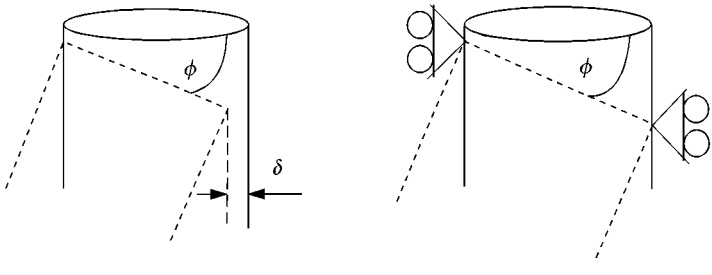


Figure 2. Discrepancy introduced for simply supported edge condition (exaggerated).

The simple supports constrain the cylinder with respect to sway and no contribution from a rigid-body mode to $Y_{Mw}^{22,23}$ occurs.

For a cylinder of dimension $L/a = 1$ and wall thickness of $h_{cyl}/a = 0{\cdot}01$, the magnitude of the axial force input mobility $Y_{Fv}^{22}(= Y_{Fv}^{33})$ is shown in Figure 3. The mobility is normalized with respect to that of an infinite plate of thickness equal to that of the cylinder wall since for point excitation in the radial direction the high-frequency behaviour of a cylinder approaches that of an infinite plate [6]. The normalized mobility is plotted versus $k_{Lcyl}a$ and, to allow comparison with a top-plate of equal thickness and radius, it is plotted versus $k_{Btop}a$ also.

For $n = 0$, a mass-controlled region is followed by an anti-resonance and this is first followed by a beam-controlled resonant region and later by a plate-controlled resonant region. A similar format is also seen for other values of $n$ though for these, because there is no associated rigid-body mode, the behaviour prior to the beam region is stiffness controlled.

Whilst the transition from beam-to plate-controlled behaviour is known to occur at the cylinder ring frequency, $k_{Lcyl}a = 1$, which, of the cylinders dimensions only involves the radius, the onset of the beam-controlled region, and thus essentially of resonant behaviour, is dependent upon all of the dimensions. That the eigenfrequencies are similarly dependent means that a general modal order cannot be established in contrast to the top-plate. The frequency of the cylinder's fundamental and subsequent resonances cannot therefore be generalized. Moreover, it is seen that for the resonant region the characteristic trend of the mobility has, similarly, a dependence upon $n$ wherefore this too cannot be generalized.

Analogous to that of $Y_{Fv}^{01}$ and $Y_{Fv}^{00}$ for the top-plate, the format of the transfer mobility $Y_{Fv}^{23}$ can be expected to be as that for $Y_{Fv}^{22}$ bar so that for $n = 0$ an anti-resonance between the mass controlled and beam-like region will not be exhibited.

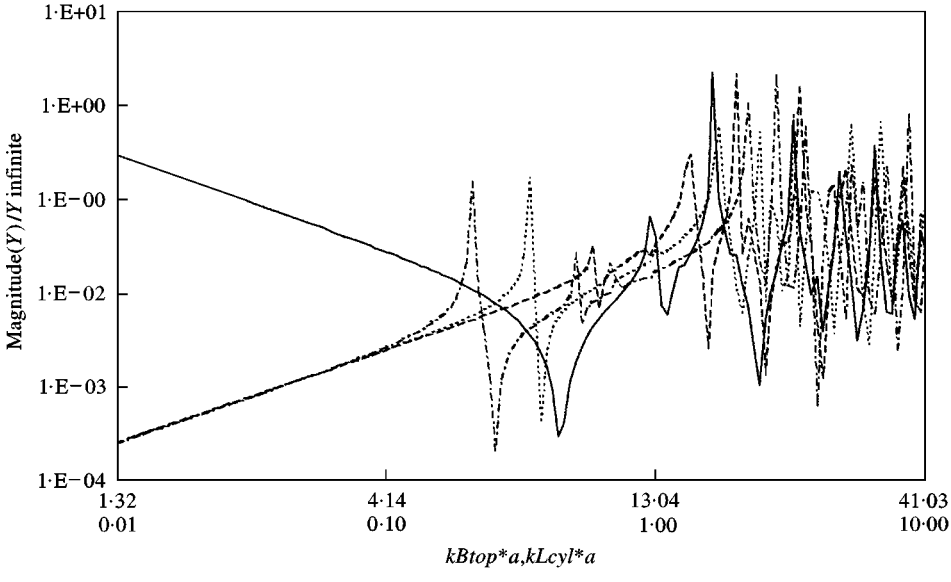


Figure 3. $Y_{vF}^{22}$ for $L/a = 1$, $h_{cyl}/a = 0{\cdot}01$. —— $n = 0$; - - - - $n = 1$; ..... $n = 2$; - · - · - $n = 3$.

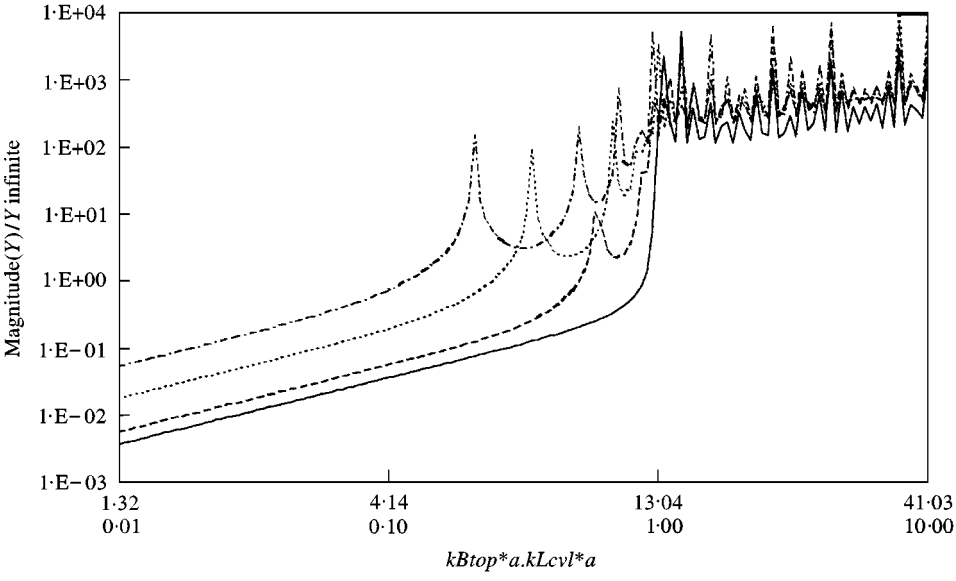


Figure 4. $Y^{23}_{Mw}$ for $L/a = 1$, $h_{cyl}/a = 0{\cdot}01$. —— $n = 0$; - - - - $n = 1$; ..... $n = 2$; - · - · - $n = 3$.

The magnitude of the moment transfer mobility $Y^{23}_{Mw}$ is shown in Figure 4. Since the cylinder does not have a rigid-body mode in rotation, stiffness-controlled behaviour followed by first beam and then plate-controlled resonant behaviour is seen for all $n$. As for the force mobilities, the modal order cannot be generalized wherefore the only resolved frequency is that of the ring mode. An interesting feature however is that for $n = 0$ there is a dramatic, almost step-like, transition from stiffness to plate-controlled resonant behaviour. Though for other orders of $n$ the transition is not as sharp, the slope prior to the ring frequency is consistently steep whereupon even for the case of $n = 3$ an increase of over three orders of magnitude in the decade [0·1, 1] is apparent. Such behaviour results, uniquely, from the very high rotational stiffness between the upper and lower edges of the cylinder and will therefore not be exhibited in the input moment mobility $Y^{22}_{Mw}$. It can therefore, and to support the hypothesis, be predicted that the transfer of moments across the cylinder is small for an extended region. Moreover, for a top-plate and side-wall of equal thickness the ring frequency occurs for $k_{Btop}a > 10$ wherefore this region will extend far beyond the fundamental resonance of the top-plate.

### 3.3. INFINITE RECIPIENT PLATE

For line excitation of an infinite plate, a wave approach can be used to establish the mobilities. Following then the work of Petersson [7] the force input mobility is given by

$$Y^{44}_{Fv} = \frac{\mathrm{i}\omega}{8DK_B^2}\left\{\begin{array}{c} \mathrm{J}_n(k_B r)\mathrm{J}_n(k_B r_0) - \\ \mathrm{i}\left[\mathrm{J}_n(k_B r)\mathrm{Y}_n(k_B r_0) + \dfrac{2}{\pi}\mathrm{I}_n(k_B r)\mathrm{K}_n(k_B r_0)\right] \end{array}\right\}, \tag{24}$$

and the cross mobility (obtained by differentiating once with respect to $r$) by

$$Y^{44}_{Fw} = \frac{\mathrm{i}\omega}{8DK_B^2}\left\{\begin{array}{l} \mathrm{J}_n(k_B r_0)\left(\dfrac{n}{k_B r}\mathrm{J}_n(k_B r) - \mathrm{J}_{n+1}(k_B r)\right) - \\ \mathrm{i}\left[\begin{array}{l} \mathrm{Y}_n(k_B r_0)\left(\dfrac{n}{k_B r}\mathrm{J}_n(k_B r) - \mathrm{J}_{n+1}(k_B r)\right) + \\ \dfrac{2}{\pi}\mathrm{K}_n(k_B r_0)\left(\dfrac{n}{k_B r}\mathrm{I}_n(k_B r) + \mathrm{I}_{n+1}(k_B r)\right) \end{array}\right] \end{array}\right\}. \tag{25}$$

The moment mobility, obtained by application of two opposing forces equidistant around $r_0$ followed by a first order Talyor expansion, is given by

$$Y^{44}_{Mw} = \frac{\omega}{8D}\left\{\begin{array}{l} \left(\dfrac{n}{k_B r_0}\mathrm{J}_n(k_B r_0) - \mathrm{J}_{n+1}(k_B r_0)\right)^2 - \\ \mathrm{i}\left[\begin{array}{l} \left(\dfrac{n}{k_B r_0}\mathrm{Y}_n(k_B r_0) - \mathrm{Y}_{n+1}(k_B r_0)\right)\left(\dfrac{n}{k_B r_0}\mathrm{J}_n(k_B r_0) - \mathrm{J}_{n+1}(k_B r_0)\right) + \\ \dfrac{2}{\pi}\left(\dfrac{n}{k_B r_0}\mathrm{K}_n(k_B r_0) - \mathrm{K}_{n+1}(k_B r_0)\right)\left(\dfrac{n}{k_B r_0}\mathrm{I}_n(k_B r_0) + \mathrm{I}_{n+1}(k_B r_0)\right) \end{array}\right] \end{array}\right\}. \tag{26}$$

For $n = 0$, the mobility follows the characteristic point mobility until approximately $k_{Brec}a = 1$ after which, the mobility has a spatial dependence because the wavelength becomes small with respect to the annular interface and a series of minima results. For the other orders of $n$, and clearly as a consequence of the force distribution being essentially moment-like, a stiffness-like slope is exhibited to $k_{Brec}a = 1$. In this region, the magnitude decreases significantly as $n$ increases indicating that the mobility is dominated by zeroth order excitation.

## 4. CAN UPON INFINITE PLATE

Using the mobilities established as ingredients, equations (2)–(9) can be implemented. Consider a can of dimension $L/a = 1$, $h_{cyl}/a = 0{\cdot}01$, $h_{top}/a = 0{\cdot}01$ attached to a recipient of dimension $h_{top}/a = 1$.[†] For an excitation force of order $n = 0$ positioned at $r_0/a = 0{\cdot}5$, the active input power, defined as

$$W = \mathrm{Re}\{Q\}, \tag{27}$$

is shown in Figure 5 for both the complete model $W_{com}$ and the reduced model $W_{red}$. Normalization is with respect to the power for a point force applied directly to the

[†]A "thick" recipient was initially selected to enable comparisons with previous work [8].

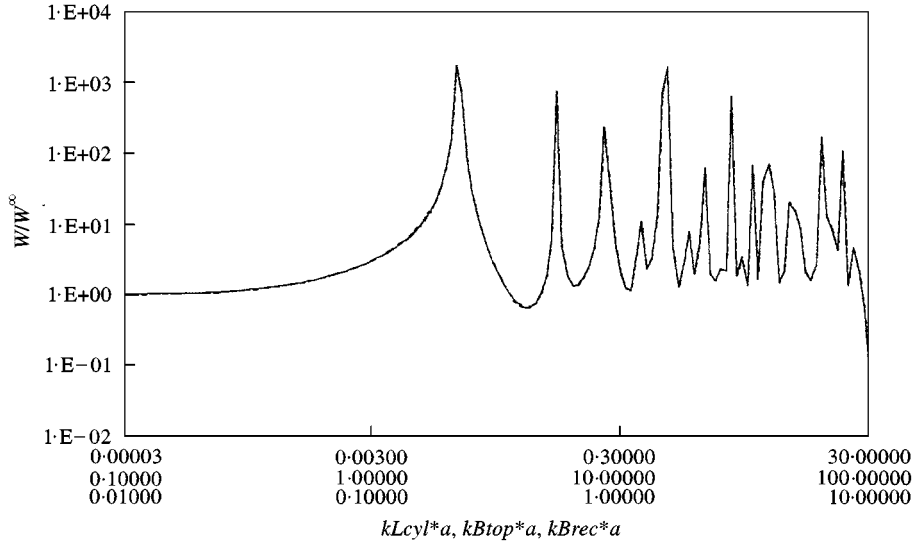


Figure 5. Input power for $n = 0$, $h_{top}/a = 0{\cdot}01$, $h_{cyl}/a = 0{\cdot}01$, $h_{rec}/a = 1$, $L/a = 1$, $r_0/a = 0{\cdot}5$. —— $w_{com}$; - - - - - $w_{red}$.

recipient plate. It is seen that the power calculated from the reduced model maps that from the complete for the entire range of Helmholtz numbers considered. This results because for $n = 0$ the applied force distribution is a uniform ring, symmetrically positioned upon the top-plate whereupon only translational force can be imparted into the side-walls.

For $n = 1$, both moments and forces can be transmitted to the side-walls and discrepancies between the two calculations are introduced, see Figure 6. In the stiffness-controlled region (occurring primarily due to the response of the recipient) the power is seen to be greater for the reduced model than for the complete one. Both the fundamental and the second resonances occur at a lower Helmholtz number for the reduced model. The positions of the higher resonances are however comparable for both models.

Since for the spatial domain the line mobilities have been formulated with a circular dependence, a Fourier series expansion and then summation of the input force allows the prominent case of point force excitation to be studied.[†] The real and imaginary parts of the input power are shown in Figures 7 and 8 respectively. For these figures, the reduced model is seen to mimic the complete model for Helmholtz numbers to the second resonance. At the second resonance, discrepancies are however seen such that for the reduced calculation the second resonance occurs at a lower Helmholtz numbers. Since superposition holds with

[†]The only difficulty with this approach is the number of modes required in the series so to attain convergence of solution. For high Helmholtz numbers, it was found that numbers in excess of 900 and 1500 modes were needed for the top-plate and cylinder respectively. For the salient physics of the system, the details of the higher resonances are however of limited significance and rather than including a high number of modes in the analysis, the upper Helmholtz number of interest can instead be reduced from $k_{Brec}a = 10$ to $k_{Brec}a = 1$.

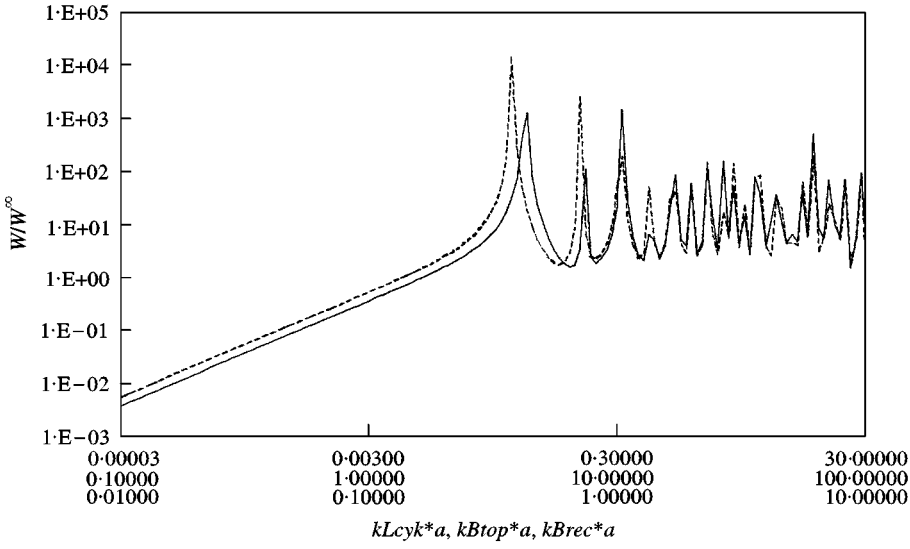


Figure 6. Input power for $n = 1$, $h_{top}/a = 0{\cdot}01$, $h_{cyl}/a = 0{\cdot}01$, $h_{rec}/a = 1$, $L/a = 1$, $r_0/a = 0{\cdot}5$. —— $w_{com}$; - - - - - $w_{red}$.

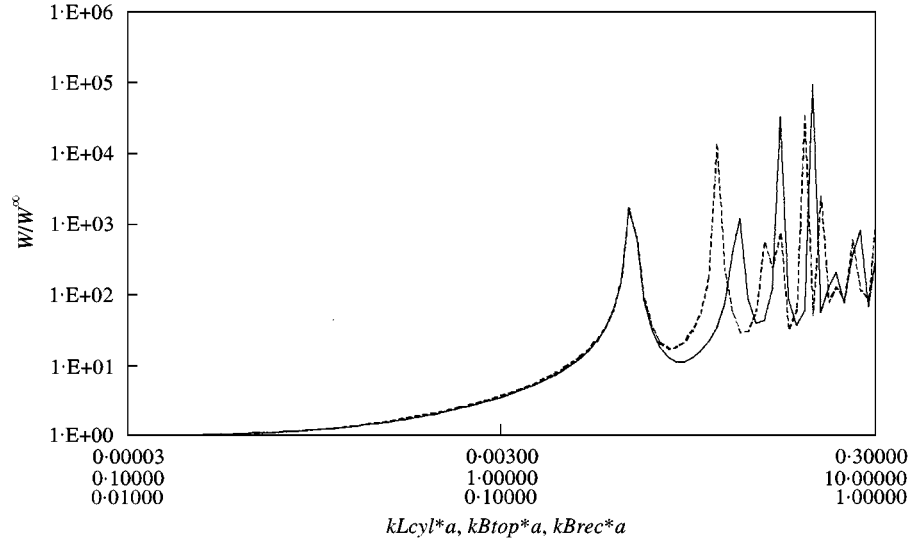


Figure 7. Real part of input power for point excitation, $h_{top}/a = 0{\cdot}01$, $h_{cyl}/a = 0{\cdot}01$, $h_{rec}/a = 1$, $L/a = 1$, $r_0/a = 0{\cdot}5$. —— $w_{com}$; - - - - - $w_{red}$.

respect to $n$, comparisons of Figure 7 with Figures 5 and 6 reveal, respectively, that the fundamental resonance is, essentially, controlled by the $n = 0$ excitation order and the second by the $n = 1$ order. It is suggested therefore that the first resonance is controlled only by the force exerted upon the side-walls whilst the second resonance is controlled by both the moment and the force. That none of the higher resonances match for both models, reveals that these too are controlled by both force and moment.

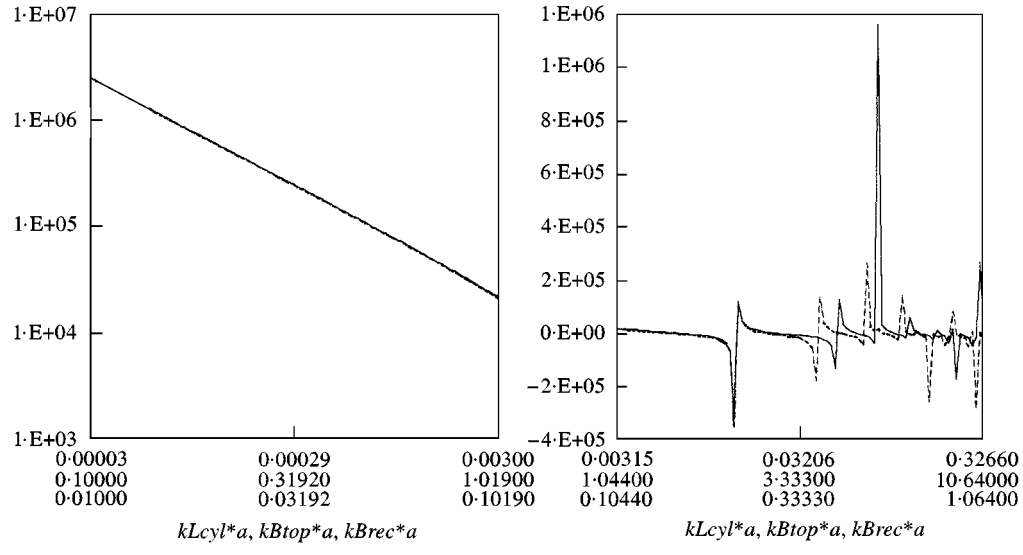


Figure 8. Imaginary part of input power for point excitation, $h_{top}/a = 0{\cdot}01$, $h_{cyl}/a = 0{\cdot}01$, $h_{rec}/a = 1$, $L/a = 1$, $r_0/a = 0{\cdot}5$. —— $w_{com}$; - - - - - $w_{red}$.

Concentrating upon the second resonance, it can be determined from the substructure mobilities that it occurs where the cylinder is stiffness controlled, i.e., for Helmholtz number $k_{Btop}a < 4 = k_{Lcyl}a < 0{\cdot}05$ and where the receiver can be likened to a point excited infinite plate, *i.e.*, $k_{Brec}a < 1$. Since for these conditions neither the cylinder nor the recipient exhibits resonance-controlled behaviour nor too, will the mobilities be conjugated, it follows that the resonance is determined only by the dimensions of the top-plate and the boundary conditions imposed upon it.

### 4.1. INFLUENCE OF UPPER BOUNDARY CONDITION

To investigate the influence of the upper boundary condition, the thickness of the top-plate relative to the side-walls can be altered. For $h_{cyl}/a = 0{\cdot}1$ and $h_{top}/a = 0{\cdot}001$, Figure 9 shows the real part of the input power for point excitation. Whilst a comparison of Figures 7 and 9 reveals that for both cases the second resonance occurs at a lower Helmholtz number for the reduced model than for the complete model, the discrepancy is largest where the thickness of the side-walls is greater than that of the top-plate, i.e., Figure 9.

For the other extreme of boundary conditions, i.e., a thick top-plate and thin cylinder walls, see Figure 10, the complete and reduced models are seen to be comparable for the whole, extended range considered.

Where the top-plate is thicker than the side-walls, the reduced model is therefore an accurate representative of the complete whilst where the cylinder walls are of comparable or of greater thickness, discrepancies between the two models occur above the fundamental resonance.

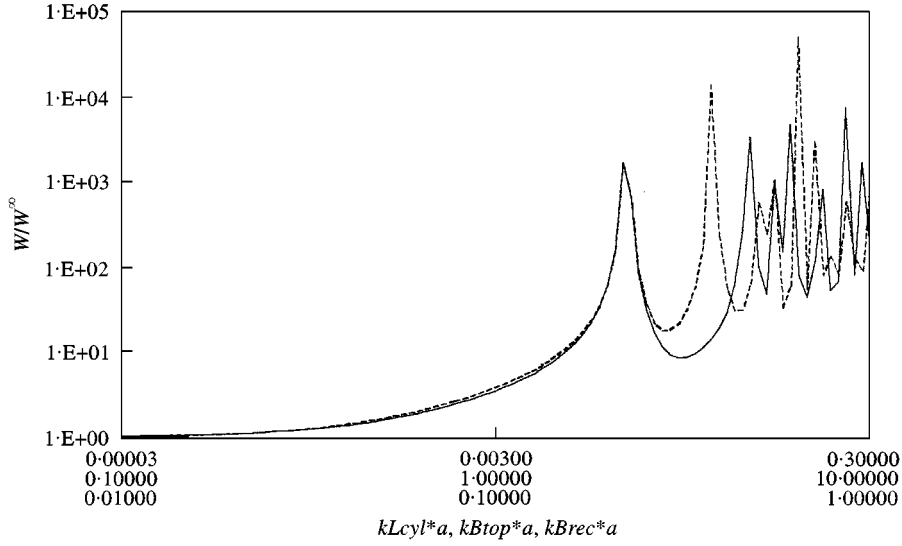


Figure 9. Real part of input power for point excitation, $h_{top}/a = 0{\cdot}01$, $h_{cyl}/a = 0{\cdot}1$, $h_{rec}/a = 1$, $L/a = 1$, $r_0/a = 0{\cdot}5$. —— $w_{com}$; - - - - - $w_{red}$.

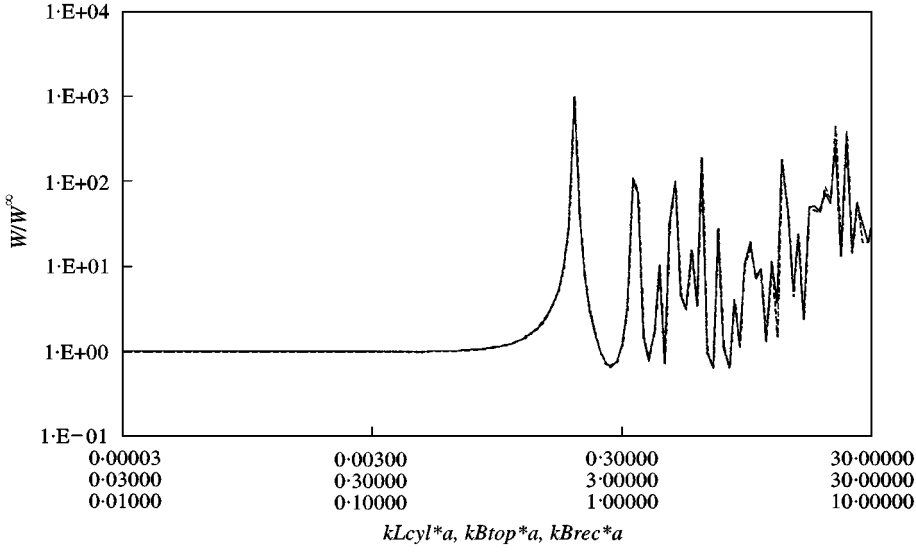


Figure 10. Real part of input power for point excitation, $h_{top}/a = 0{\cdot}1$, $h_{cyl}/a = 0{\cdot}01$, $h_{rec}/a = 1$, $L/a = 1$, $r_0/a = 0{\cdot}5$. —— $w_{com}$; - - - - - $w_{red}$.

To explain this sensitivity to the top-plate/side-wall interface the following argument applies. For a thick top-plate, the rotation at the interface is dictated by the plate characteristics and the restoring moments from the thin side-walls can be neglected. This means that the reduced model is an adequate representation of the complete. However, where, the top-plate is thin and the walls thick, the rotation is governed by the latter wherefore, for the reduced model, in which the restoring

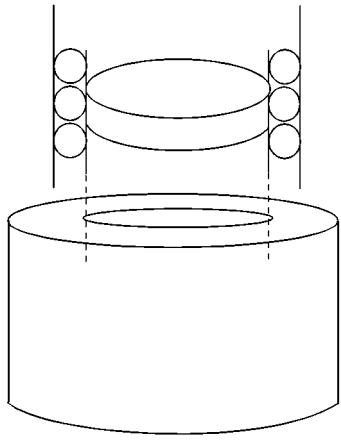

Figure 11. Guided top-plate fitted inside the cylinder.

moments are neglected, those resonances influenced by moments occur at lower Helmholtz numbers than those obtained with the complete model.

It follows that in order to account for such an effect, a rotational constraint can be introduced "artificially" into the reduced model. Whilst retaining the simplified formulation this can be achieved by considering the boundary condition of the top-plate to be guided instead of being free along the edge, see Figure 11. Further compatibility is also achieved by assuming that the top-plate dimension is such that it fits inside the cylinder walls. It is appropriate to introduce rotational stiffness for all orders of $n$ other than $n = 0$. The exception being so because for $n = 0$ as seen in Figure 5, the cylinder is not excited with respect to rotation and the rotational stiffness has therefore no influence. For $n = 0$, the free edge condition should therefore be retained. Also, the two rigid-body modes have to be maintained since the guided condition is relative to the cylinder walls and not global.

For the case of $h_{cyl}/a = 0{\cdot}1$, Figure 12(a) is produced. The compatibility of the reduced and complete models is seen to be restored, cf. Figure 9. Where differences in amplitude are seen, the limited frequency resolution offers an explanation, whereby the calculation omits the "absolute position" of the resonance. This is demonstrated in Figure 12(b) for which the upper range of Figure 12(a) is shown recalculated with a much refined frequency resolution. Not only is the compatibility of the resonance peaks improved but moreover, considering the first four, there is no consistency between over or under-estimation. Therefore this means that "care" has to be taken when determining the maximum of the resonance peaks in a narrow-band calculation. In frequency-averaged applications, for example third octave band, this is clearly less critical.

Application of the guided top-plate model to the case where both $h_{top}/a$ and $h_{cyl}/a = 0{\cdot}01$ is, however, less successful, see Figure 13. It is seen that those resonances for which the moment is influential are at higher Helmholtz number for the guided model, $W_{gui}$, than for the complete model.This indicates therefore that the guided model is stiffer than the complete model. Moreover, because the guided model can be considered to represent a limiting case, its applicability can be

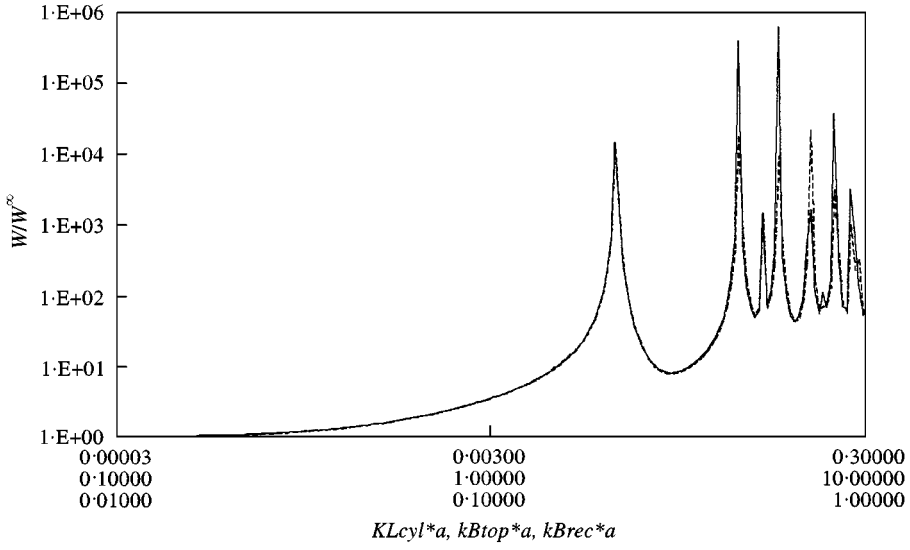


Figure 12(a). Input power for point excitation where the geometry is such that the top-plate is inside the cylinder, $h_{top}/a = 0{\cdot}01$, $h_{cyl}/a = 0{\cdot}1$, $h_{rec}/a = 1$, $L/a = 1$, $r_0/a = 0{\cdot}5$. —— $w_{com}$; - - - - - $w_{gui}$.

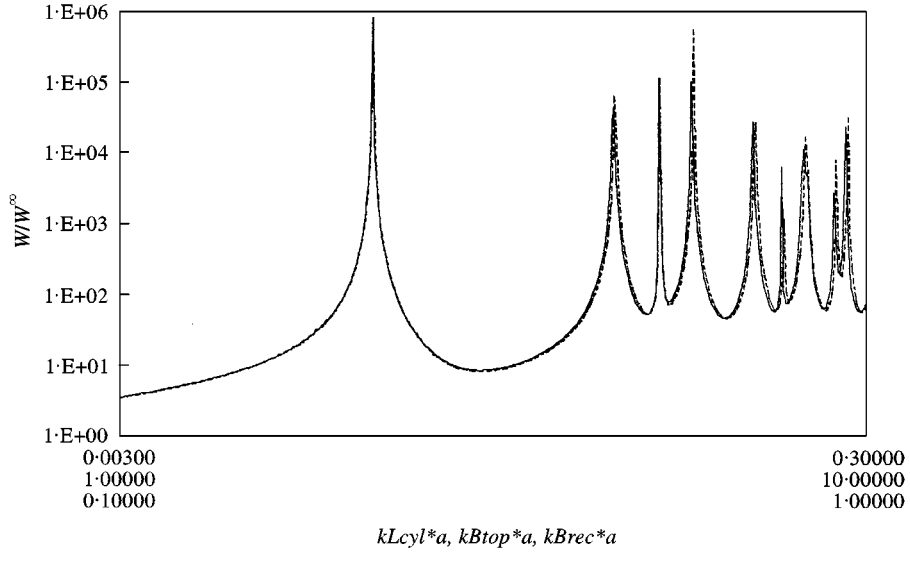


Figure 12(b). The upper part of Figure 12(a) calculated with a much finer resolution. —— $w_{com}$; - - - - - $w_{gui}$.

expected to decrease as the ratio of cylinder thickness to top-plate thickness decreases. It is shown therefore that where the top-plate and side-wall are of equal thickness is the "worst-case scenario". Moreover, understanding the significance of the top-plate and side-wall thickness poses an investigation of the criterion for the distinction of thick and thin top-plates and side-walls.

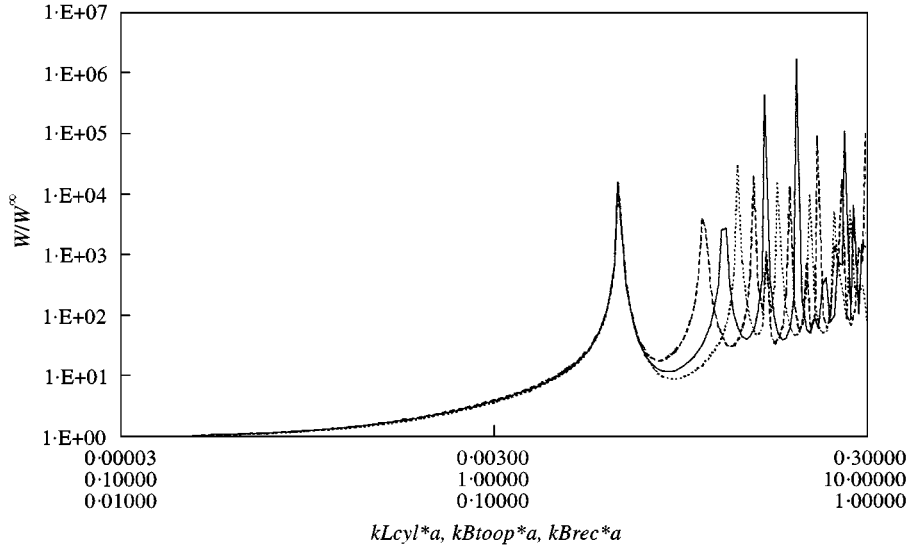


Figure 13. Input power for point excitation, $h_{top}/a = 0{\cdot}01$, $h_{cyl}/a = 0{\cdot}01$, $h_{rec}/a = 1$, $L/a = 1$, $r_0/a = 0{\cdot}5$. —— $w_{com}$; - - - - - $w_{red}$; ..... $w_{gui}$.

To compare with Figures 7 and 10, results are shown in Figure 14 for cases where $h_{cyl}/h_{top}$ is 1·5, 2, and 2·5 respectively. With respect to the resonance frequencies, discrepancies between the complete and reduced model are thereby deemed negligible where the ratio is 2 or greater.

To compare with Figures 9 and 12, results are also shown for $h_{top}/h_{cyl} = 1{\cdot}5$, 2, and 2·5, see Figure 15. Again, the discrepancies between the complete and reduced model can be considered negligible where the ratio is 2 or greater.

All the results suggest therefore a 'rule-of-thumb' whence a structure can be considered 'thick' if its thickness is twice that of another.

### 4.2. INFLUENCE OF LOWER BOUNDARY CONDITION

As for the upper boundary, the influence of the lower boundary condition can be assessed by varying the relative thickness of the two coupled structures. Hence, assuming that the least-favourable condition is where the recipient plate is of equal thickness to the side-walls, models are considered in which $h_{rec}/a = h_{cyl}/a = 0{\cdot}01$. The input power is calculated where the top-plate has dimension $h_{top}/a = 0{\cdot}02$, see Figure 16, and where $h_{top}/a = 0{\cdot}005$, see Figure 17. The complete and reduced calculations are seen to be comparable for both situations. Clearly, therefore, the influence of the moment at the lower boundary is negligible.

### 4.3. INFLUENCE OF DIMENSIONS

To investigate how the two reduced models compare with the complete model for changes of relationship between radius and length, two systems of "extreme"

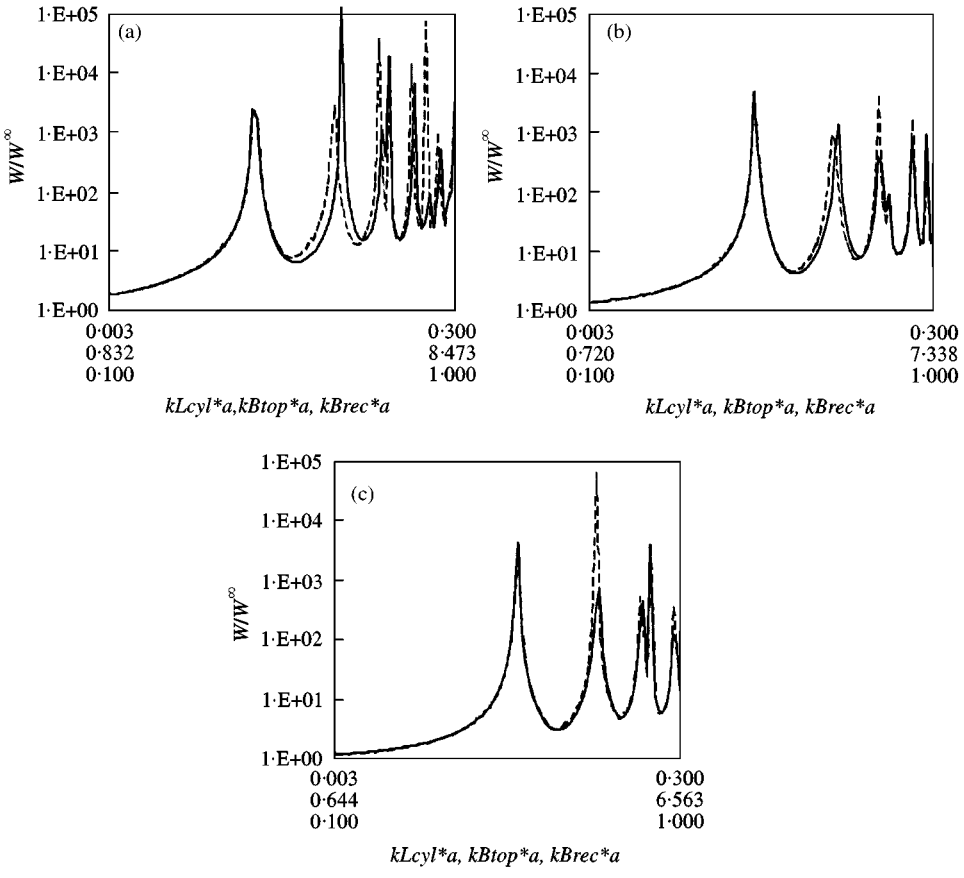


Figure 14. Input power for point excitation, $h_{cyl}/a = 0{\cdot}01$, $h_{rec}/a = 1$, $L/a = 1$, $r_0/a = 0{\cdot}5$. (a) $h_{top}/a = 0{\cdot}015$, (b) $h_{top}/a = 0{\cdot}02$, (c) $h_{top}/a = 0{\cdot}025$. —— $w_{com}$; - - - - - $w_{red}$.

conditions were considered, $L/a = 5$ and 0·2. For point excitation at $r_0/a = 0{\cdot}5$ and with $h_{top}/a = 0{\cdot}01$ and $h_{cyl}/a = 0{\cdot}02$ the resultant calculation of the input power is shown in Figures 18 and 19. For both cases, $W_{gui}$ is an accurate representation of $W_{com}$.

For extreme radii, the condition of $h_{top}/a = 0{\cdot}004$ and $h_{cyl}/a = 0{\cdot}002$ is also considered, see Figures 20 and 21. Again $W_{red}$ and $W_{com}$ are seen to be comparable over the whole range.

Physically, these comparisons demonstrate the weak interplay between the top-plate thickness and radius with respect to the bending stiffness and influence of the rotational constraints at the boundary.

### 4.4. POWER TRANSMISSION AT LOWER INTERFACE

In addition to the input power, the power transmitted through a built-up structure and into its surroundings is also of interest for engineering design. For the cylindrical can, this is represented by the power at the lower interface. Since within

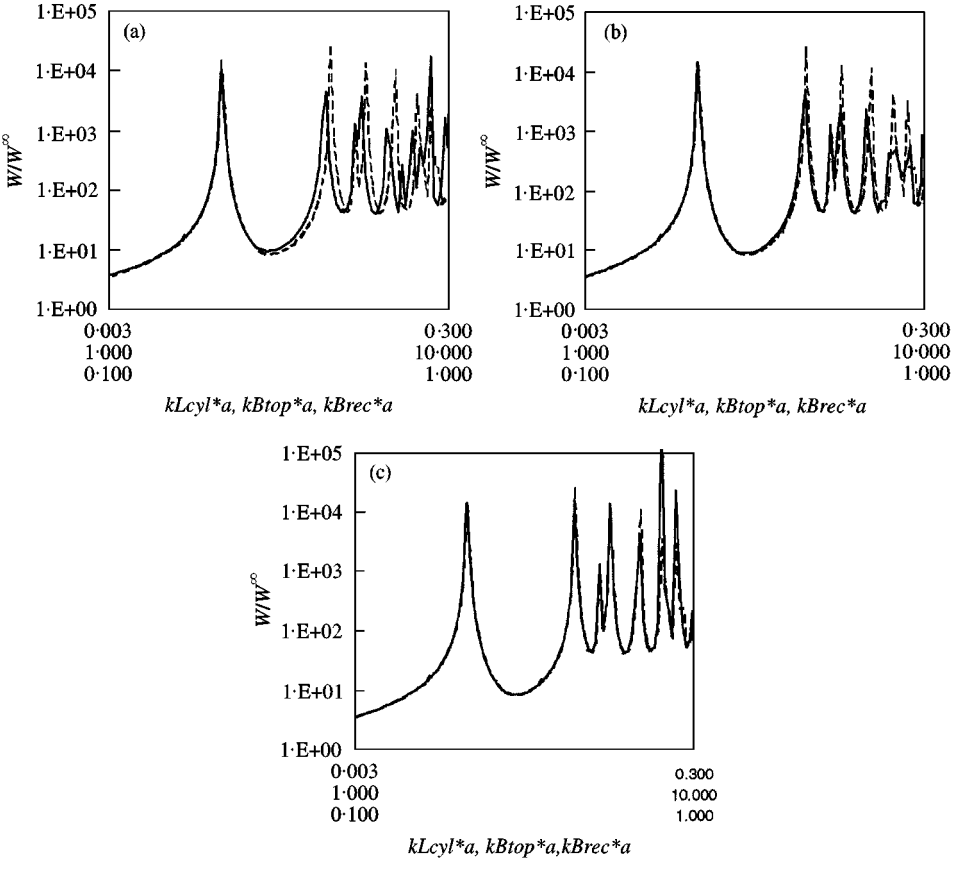


Figure 15. Input power for point excitation, $h_{cyl}/a = 0{\cdot}01$, $h_{rec}/a = 1$, $L/a = 1$, $r_0/a = 0{\cdot}5$. (a) $h_{top}/a = 0{\cdot}015$, (b) $h_{top}/a = 0{\cdot}02$, (c) $h_{top}/a = 0{\cdot}025$. —— $w_{com}$; - - - - - $w_{gui}$.

the side-walls any conversion from force-induced power to moment-induced power can be expected to be small, similar findings with respect to compatibility of the complete and reduced models can be expected to hold for both the power at the input and at the lower interface. As an illustration, the power at the lower interface is shown in Figure 22 for $L/a = 1$ and with both $h_{top}/a$ and $h_{cyl}/a = 0{\cdot}001$. The discrepancies between the reduced and complete models are indeed seen to be comparable to those of the corresponding input power plots, i.e., compare Figure 22 with 13. The same is true when the recipient plate is of thickness equal to that of the side-walls, see Figures 23 and compare with Figure 16.

### 4.5. INFLUENCE OF FORCE LOCATION

In addition to the system dimensions, the power will also be influenced by the eccentricity of the force. A force at the centre for example, constituents a symmetric loading such that there will be no global moment excitation of the cylinder and $W_{red}$ can be expected to be comparable to $W_{com}$ for all conditions.

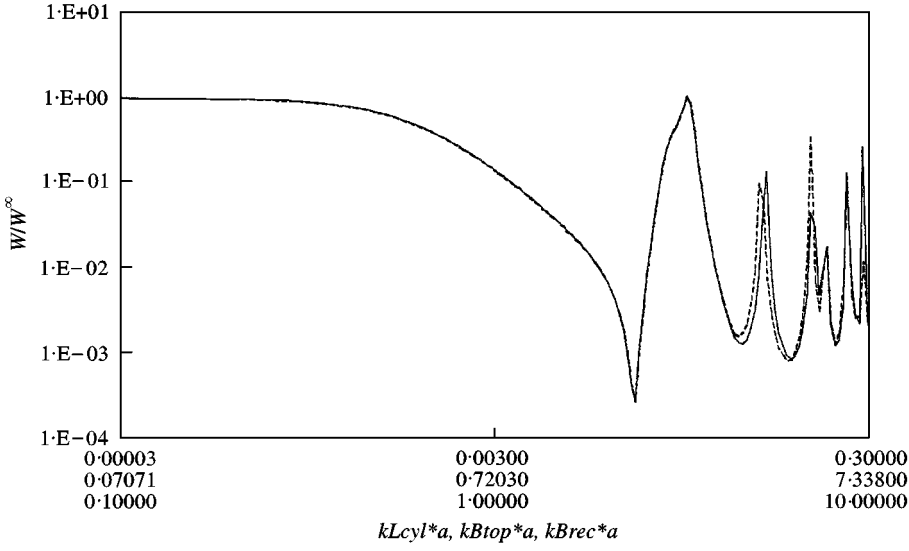


Figure 16. Input power for point excitation, $h_{top}/a = 0{\cdot}02$, $h_{cyl}/a = 0{\cdot}01$, $h_{rec}/a = 0{\cdot}01$, $L/a = 1$, $r_0/a = 0{\cdot}5$. —— $w_{com}$; - - - - - $w_{red}$.

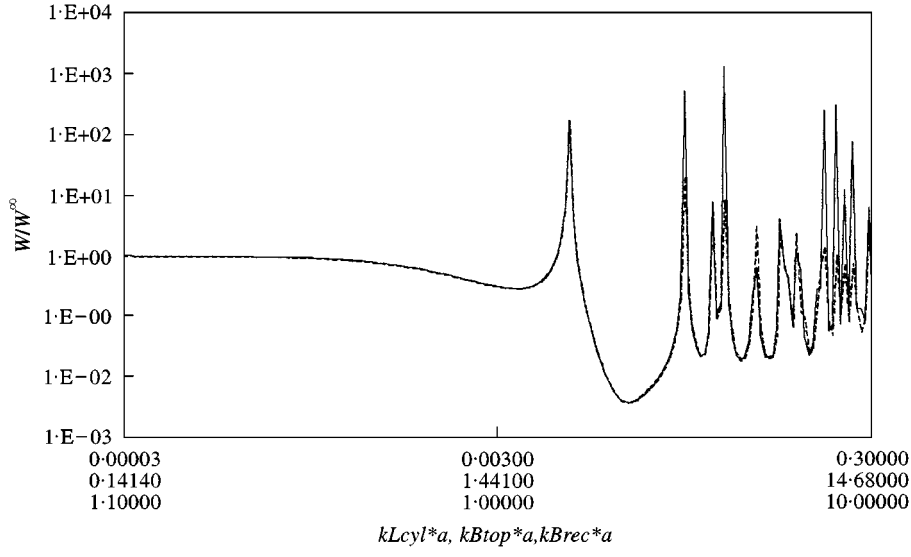


Figure 17. Input power for point excitation, $h_{top}/a = 0{\cdot}005$, $h_{cyl}/a = 0{\cdot}01$, $h_{rec}/a = 0{\cdot}01$, $L/a = 1$, $r_0/a = 0{\cdot}5$. —— $w_{com}$; - - - - - $w_{gui}$.

With $L/a = 1$ and both $h_{top}/a$ and $h_{cyl}/\mathrm{a} = 0{\cdot}01$, the power at the lower interface is considered for point forces positioned at $r_0/a = 0{\cdot}3$ and $0{\cdot}9$, see Figures 24 and 25. The discrepancies between the reduced model and the complete are similar for both figures and are comparable to the case of $r_0/a = 0{\cdot}5$, i.e., Figure 22.

It is interesting to observe that for $r_0/a = 0{\cdot}9$ sharp drops in the power occurs. At these frequencies, the force position can be shown to almost coincide with a nodal

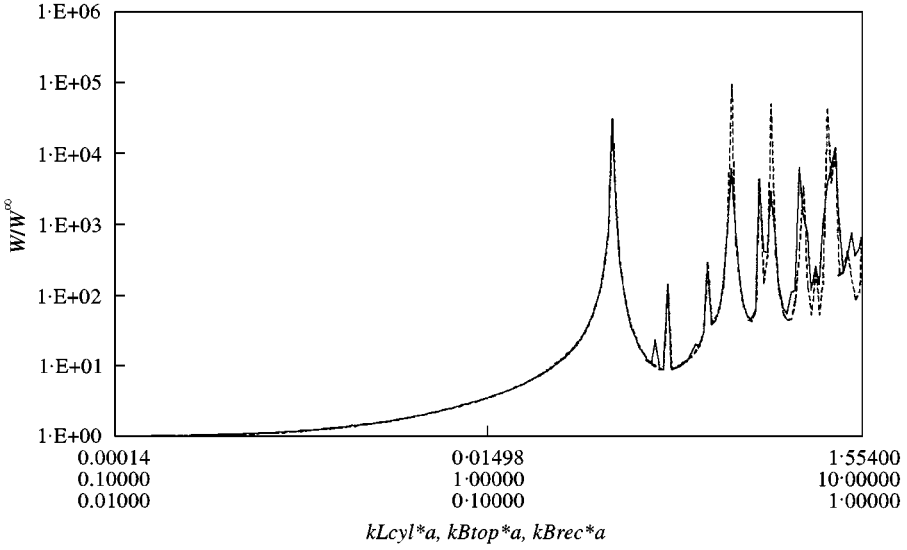


Figure 18. Input power for point force, $h_{top}/a = 0{\cdot}05$, $h_{cyl}/a = 0{\cdot}1$, $h_{rec}/a = 5$, $L/a = 25$, $r_0/a = 0{\cdot}5$. —— $w_{com}$; - - - - - $w_{gui}$.

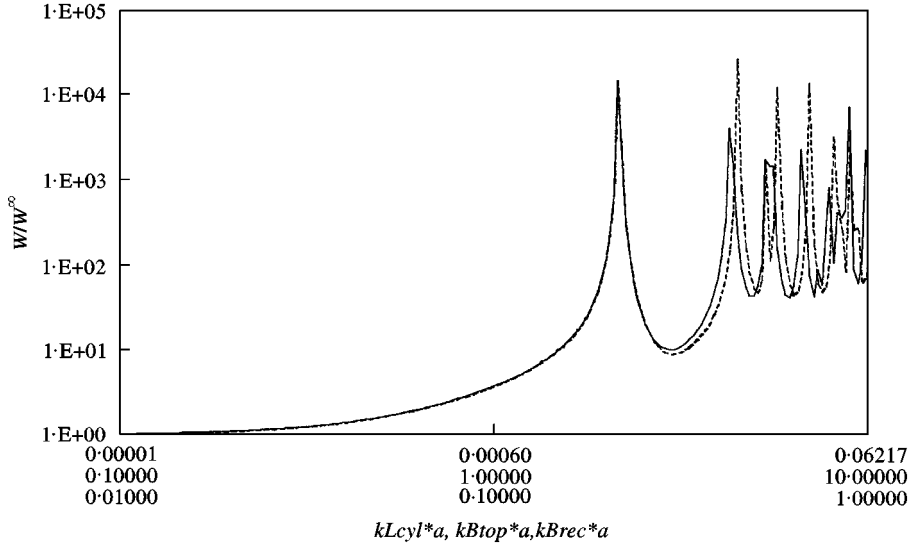


Figure 19. Input power for point force, $h_{top}/a = 0{\cdot}002$, $h_{cyl}/a = 0{\cdot}004$, $h_{rec}/a = 0{\cdot}2$, $L/a = 0{\cdot}2$, $r_0/a = 0{\cdot}5$. —— $w_{com}$; - - - - - $w_{gui}$.

line whereupon the system is weakly excited. The physics of these minima is therefore not unique to the condition of a force close to the edge and for other force positions minima can likewise be expected. At higher frequencies, the influence of dissipation, however, is such that they are less pronounced, see Figure 24 at $k_{Brec}a \approx 0{\cdot}8$.

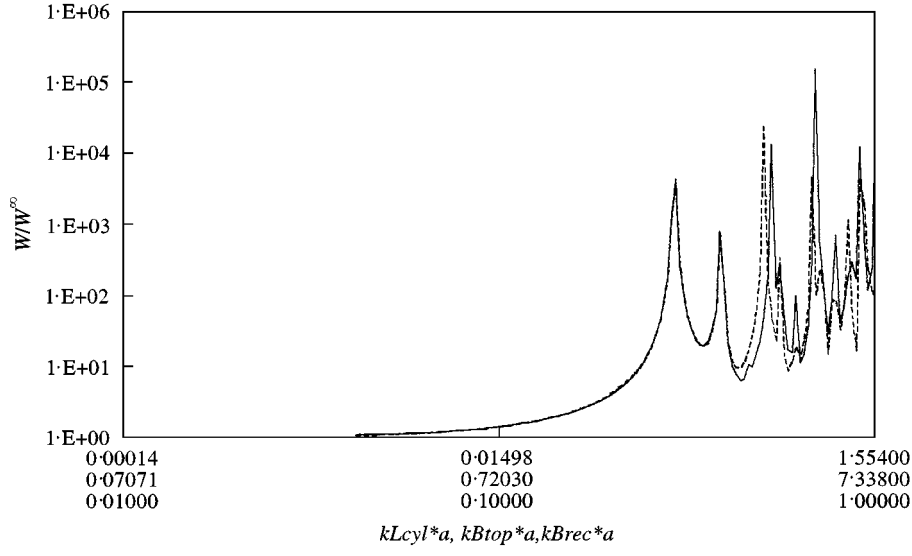


Figure 20. Input power for point force, $h_{top}/a = 0{\cdot}1$, $h_{cyl}/a = 0{\cdot}05$, $h_{rec}/a = 5$, $L/a = 5$, $r_0/a = 0{\cdot}5$. —— $w_{com}$; - - - - - $w_{red}$.

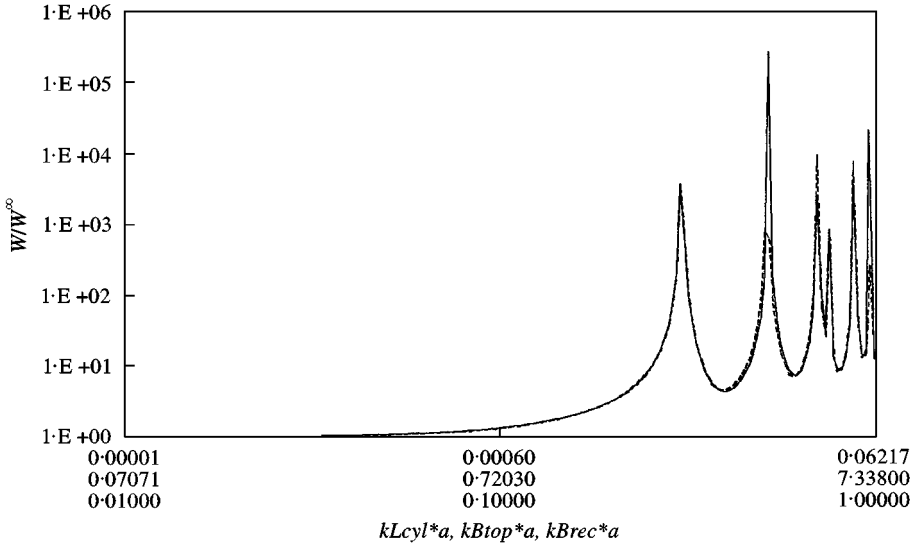


Figure 21. Input power for point force, $h_{top}/a = 0{\cdot}004$, $h_{cyl}/a = 0{\cdot}002$, $h_{rec}/a = 0{\cdot}2$, $L/a = 0{\cdot}2$, $r_0/a = 0{\cdot}5$. —— $w_{com}$; - - - - - $w_{red}$.

### 4.6. FURTHER SIMPLIFICATION OF MODEL

From Figure 3, it is known, for the typical dimensions considered, that over much of the Helmholtz number range, the cylinder acts, with respect to force excitation, as either a mass ($n = 0$) or as a stiffness ($n > 0$). Where it is mass-like, the point and transfer mobilities will clearly be equal. Under the condition of "long" wavelengths, approximations can also be found when its behaviour is stiffness-like.

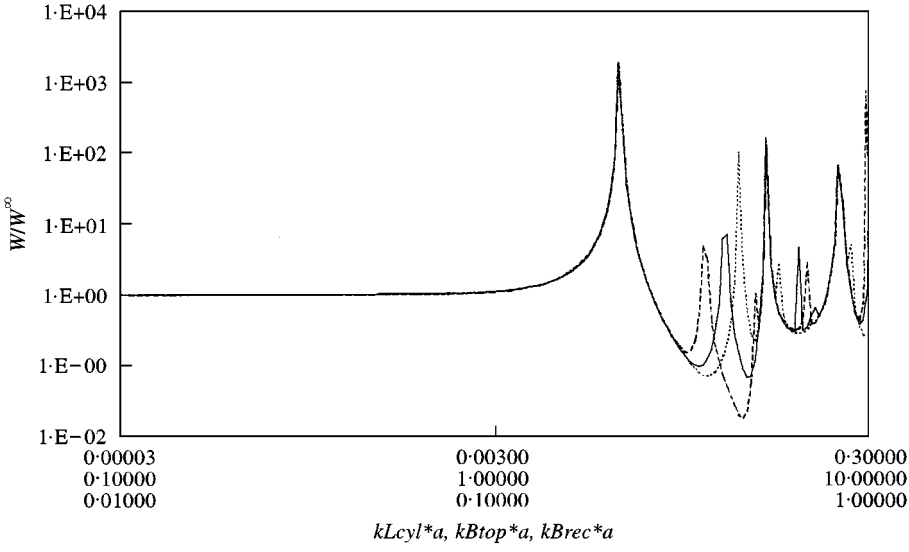


Figure 22. Power at lower interface for point force, $h_{top}/a = 0{\cdot}01$, $h_{cyl}/a = 0{\cdot}01$, $h_{rec}/a = 1$, $L/a = 1$, $r_0/a = 0{\cdot}5$. —— $w_{com}$; - - - - - $w_{red}$; ..... $w_{gui}$.

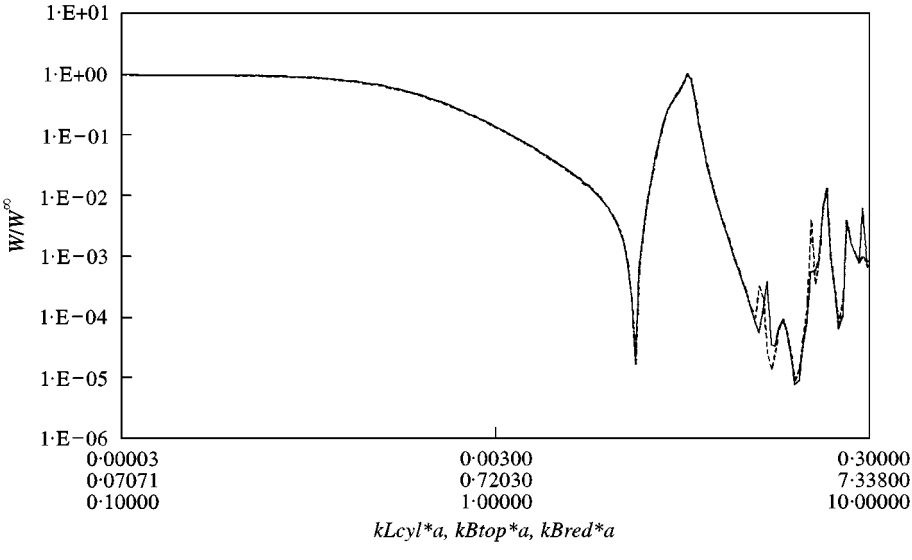


Figure 23. Power at lower interface for point force, $h_{top}/a = 0{\cdot}02$, $h_{cyl}/a = 0{\cdot}01$, $h_{rec}/a = 0{\cdot}01$, $L/a = 1$, $r_0/a = 0{\cdot}5$. —— $w_{com}$; - - - - - $w_{red}$.

Assuming these two conditions and that the recipient is "rigid" compared with the cylinder ($Y_{Fv}^{22} > Y_{Fv}^{44}$) and so acts as a point-excited structure, permits the reduced model to be simplified.

The active, transmitted power at the input position becomes

$$W = \frac{1}{2}\,\mathrm{Re}\left\{Y_{Fv}^{00} + \frac{Y_{Fv}^{01}Y_{Fv}^{01}}{(Y_{Fv}^{11} + Y_{Fv}^{44})}\right\}|F_0|^2, \tag{28}$$

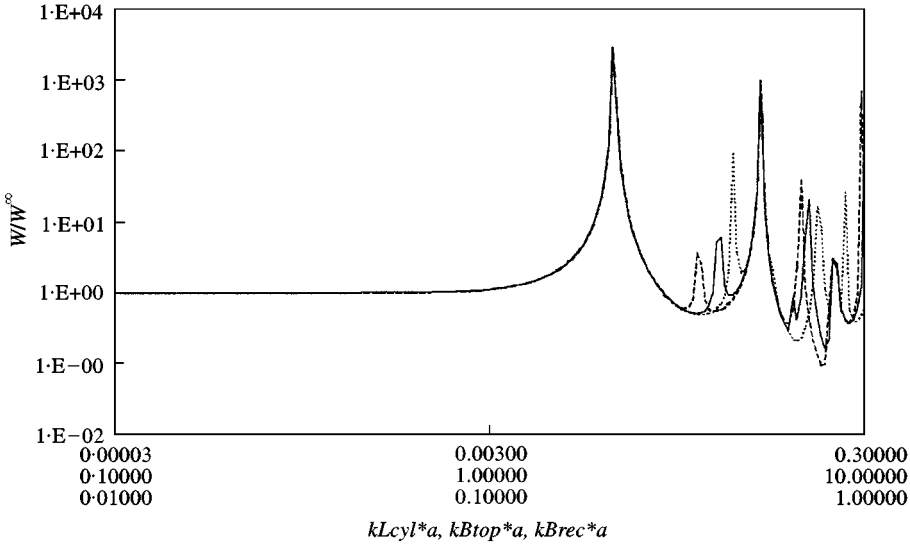


Figure 24. Power at lower interface for point force, $h_{top}/a = 0{\cdot}01$, $h_{cyl}/a = 0{\cdot}01$, $h_{rec}/a = 1$, $L/a = 1$, $r_0/a = 0{\cdot}3$. —— $w_{com}$; - - - - - $w_{red}$; ..... $w_{gui}$.

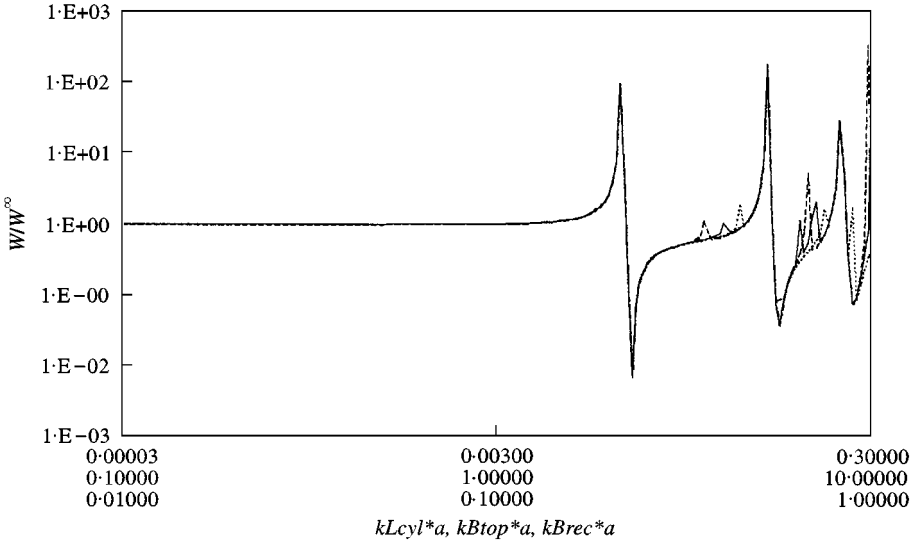


Figure 25. Power at lower interface for point force, $h_{top}/a = 0{\cdot}01$, $h_{cyl}/a = 0{\cdot}01$, $h_{rec}/a = 1$, $L/a = 1$, $r_0/a = 0{\cdot}9$. —— $w_{com}$; - - - - - $w_{red}$; ..... $w_{gui}$.

and at the lower interface simply,

$$W = \frac{1}{2}\mathrm{Re}\{Y_{Fv}^{44}\}\frac{|Y_{Fv}^{01}|^2}{|Y_{Fv}^{11}|^2}|F_0|^2\,. \tag{29}$$

A comparison of the results forthcoming from these expressions with those from the reduced model allows an examination of the cylinders influence on the power. With

both $h_{top}/a$ and $h_{cyl}/a = 0{\cdot}01$ and $L/a = 1$, a calculation of the power at the lower interface is thus shown in Figures 26 and 27 for the cases of, compared to the length, a large and a small radius respectively.

Whilst for both cases, it appears that the simplified calculation $W_{sim}$ is a useful approximation of the reduced model this is seen to be more so for a large radius than for a small radius. Clearly, this can be expected since for the limiting case of

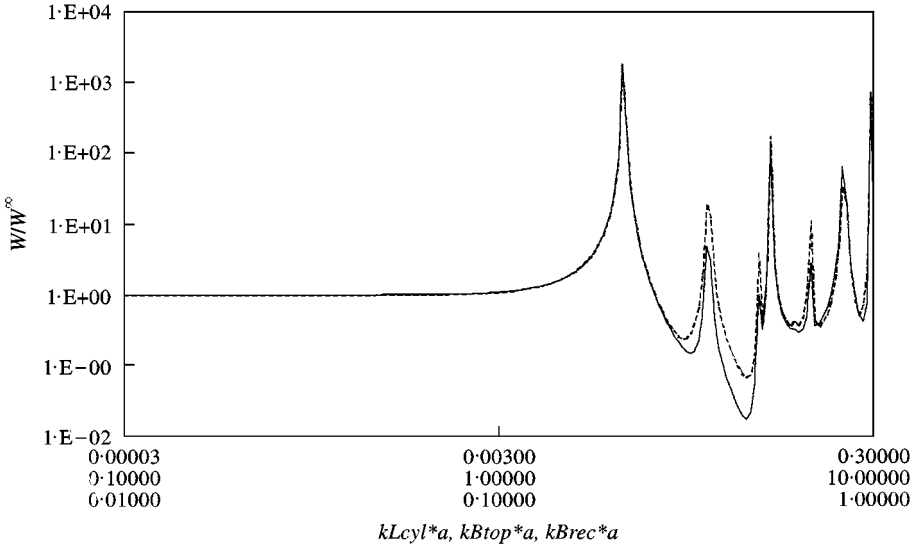


Figure 26. Power at lower interface for point force, $h_{top}/a = 0{\cdot}01$, $h_{cyl}/a = 0{\cdot}01$, $h_{rec}/a = 1$, $L/a = 1$, $r_0/a = 0{\cdot}5$. —— $w_{red}$; - - - - - $w_{sim}$.

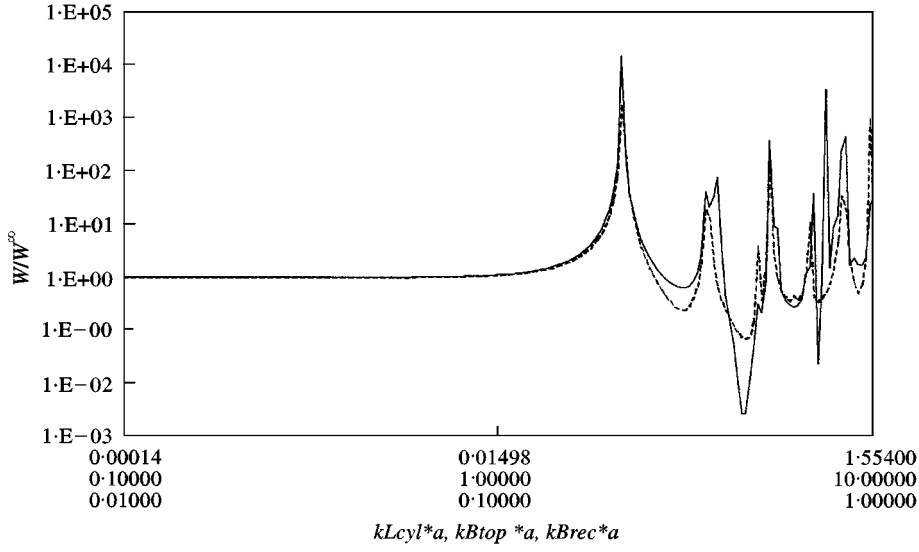


Figure 27. Power at lower interface for point force, $h_{top}/a = 0{\cdot}05$, $h_{cyl}/a = 0{\cdot}05$, $h_{rec}/a = 5$, $L/a = 4$, $r_0/a = 0{\cdot}5$. —— $w_{red}$; - - - - - $w_{sim}$.

$a \to 0$, the system will become rod-like and accordingly dominated by the cylinder behaviour, cf. reference [9].

Finally, it is noteworthy that the denominator of equation (29) is the input mobility at the edge of the top-plate. The maxima seen in the transmitted power must therefore coexist with the minima, i.e., anti-resonances, of this mobility. Since the losses of the can have limited influenced upon these minima it can be noted that the maxima of the transmitted power are controlled by the losses of the recipient only. Moreover, and in contrast to a calculation of the input power (Figures 12(a, b)), it means that less "care" need be taken of the frequency resolution when performing a narrow-band calculation of the transmitted power.

## 5. CONCLUDING REMARKS

Including both translational and rotational degrees of freedom a complete analytical model of a circular can upon an infinite recipient-plate has been developed and, with respect to both the input and transmitted power, used to study the role played by the moments as the upper and lower interfaces. For all cases of typical dimension, Helmholtz number range and force position considered, it has been shown that

— where the thickness of the cans top-plate is "thin" compared with that of the side-wall the moments have limited influence and, within "engineering accuracy", can be ignored in an analysis.
— If the side-wall thickness is equal to that of the top-plate the rotational stiffness of the system is significant and the resultant moment has an influence upon frequencies above the fundamental system resonance.
— Rotational stiffness can be introduced "artificially" by imposing, with respect to rotation, a blocked boundary condition on the top-plate. Where the side-walls are "thick" compared with the top-plate this takes into account the role of the "true" moment coupling.
— The condition of "thin/thick" appears to be such that a structure can be considered thick compared with another if (and if both are the same material) the thickness ratio is two or greater.
— With respect to a simplified analysis the most unfavourable condition is where the thickness of the side-walls is equal to the top-plate. If for this condition the moment coupling is ignored, the system is too compliant. Conversely, if the rotational stiffness is introduced "artificially" the system, it is too stiff.
— For an extended frequency range, the side-walls of the can are either mass or stiffness controlled whereupon it can be assumed that the transfer mobility from the upper and lower interface of the side-walls is comparable to the input mobility. This permits the development of simple expressions for both the input and transmitted power at the lower interface.
— From these expressions, it appears that the maximum power is input into the can system at the anti-resonances of the top-plate edge mobility.
— For the model, all the above remain so, where the ratio of can radius to height is within the limits of 0·2–5.

## ACKNOWLEDGMENTS

The authors are grateful to Dr C. deJong and Mr F. v.d. Knaap, TNO Institute of Applied Physics, Netherlands, for their constructive criticism on the work.

## REFERENCES

1. R. E. D. Bishop and D. C. Johnson 1960 *The Mechanics of Vibration*, London: Cambridge University Press.
2. B. A. T. Petersson 1994 *Journal of Sound and Vibration*, **176**, 625–639. Efficiency of annually distributed moment and force excitation regarding structural acoustic power transmission to plate-like structures.
3. B. A. T. Petersson 1993 TPD-HAG-RPT-93-0215, TNO Institute of Applied Physics, Department of Ship Acoustics. Matched asymptotic mobilities — approximations for box-like seating structures.
4. A. E. H. Love 1948 *A Treatise on the Mathematical Theory of Elasticity*. New York: Dover Publications.
5. W. Soedel 1981 *Vibrations of Shells and Plates*. New York: Marcel Dekker.
6. M. Heckl 1962 *Journal of the Acoustical Society of America* **34**, 1553–1557. Vibrations of point-driven cylindrical shells.
7. B. A. T. Petersson 1997 *Journal of Sound and Vibration* **202**, 511–537. Geometrical and spatial effects on effective mobilities of annular interfaces.
8. E. Nijman, B. A. T. Petersson and F. Van Knaap 1992 TPD-HAG-RPT-92-201. TNO Institute of Applied Physics. Department of Ship Acoustics, An experimental study of the dynamic characteristics of full-scale ship double bottom structures.
9. B. A. T. Petterson 1991 TPD-SA-RPT-91-79, TNO Institute of Applied Physics, Department of Ship Acoustics. Mobilities of seating structures. Part I: expressions for column structures.

## APPENDIX A: DETAILS OF THE TOP-PLATE MOBILITIES

Assuming a free edge for the top-plate, the boundary conditions needed to be satisfied at $r = a$ are

$$0 = -D\left[\frac{\partial^2 U(r,\theta)}{\partial r^2} + \nu\left(\frac{1}{r^2}\frac{\partial^2 U(r,\theta)}{\partial \theta^2} + \frac{1}{r}\frac{\partial U(r,\theta)}{\partial r}\right)\right] \tag{A11}$$

and

$$0 = -D\left[\frac{\partial^3 U(r,\theta)}{\partial r^3} + \frac{1}{r}\frac{\partial^2 U(r,\theta)}{\partial r^2} - \frac{1}{r^2}\frac{\partial U(r,\theta)}{\partial r} + \frac{1}{r^2}\frac{\partial^3 U(r,\theta)}{\partial r \partial \theta^2} - \frac{2}{r^3}\frac{\partial^2 U(r,\theta)}{\partial \theta^2}\right], \tag{A1}$$

where

$$U(r,\theta) = [B_1 \mathrm{J}_n(\lambda r) + B_2(\lambda r)]\, A_1 \cos(n\theta), \tag{A3}$$

$$\frac{\partial U(r,\theta)}{\partial r} = \left[ B_1\left(\frac{n}{r}\mathrm{J}_n(\lambda r) - \lambda \mathrm{J}_{n+1}(\lambda r)\right) + B_2\left(\frac{n}{r}\mathrm{I}_n(\lambda r) + \lambda \mathrm{I}_{n+1}(\lambda r)\right)\right] A_1 \cos(n\theta), \tag{A4}$$

$$\frac{\partial^2 U(r,\theta)}{\partial r^2} = \begin{bmatrix} B_1\left(\mathrm{J}_n(\lambda r)\left\{\dfrac{n(n-1)}{r^2} - \lambda^2\right\} + \mathrm{J}_{n+1}(\lambda r)\left\{\dfrac{\lambda}{r}\right\}\right) + \\ B_2\left(\mathrm{I}_n(\lambda r)\left\{\dfrac{n(n-1)}{r^2} - \lambda^2\right\} - \mathrm{I}_{n+1}(\lambda r)\left\{\dfrac{\lambda}{r}\right\}\right) \end{bmatrix} A_1 \cos(n\theta), \tag{A5}$$

$$\frac{\partial^3 U(r,\theta)}{\partial r^3} = \begin{bmatrix} B_1\left(\begin{array}{l} \mathrm{J}_n(\lambda r)\left\{\dfrac{\lambda^2}{r}(1-n) + \dfrac{n}{r^3}(n-2)(n-1)\right\} - \\ \mathrm{J}_{n+1}(\lambda r)\left\{\dfrac{\lambda}{r^2}(n^2+2) - \lambda^3\right\} \end{array}\right) + \\ B_1\left(\begin{array}{l} \mathrm{I}_n(\lambda r)\left\{\dfrac{\lambda^2}{r}(n-1) + \dfrac{n}{r^3}(n-2)(n-1)\right\} + \\ \mathrm{I}_{n+1}(\lambda r)\left\{\dfrac{\lambda}{r}(n^2+2) + \lambda^3\right\} \end{array}\right) \end{bmatrix} A_1 \cos(n\theta) \tag{A6}$$

and

$$\frac{\partial^2 U(r,\theta)}{\partial \theta^2} = [B_1 \mathrm{J}_n(\lambda r) + B_2(\lambda r)] n^2 A_1 \cos(n\theta). \tag{A7}$$

Solving this set of equations gives the modal loci $\lambda_{mn}$ of the top-plate. The natural frequencies are related to the modal loci via

$$\omega_{mn} = \frac{(\lambda_{mn} a)^2}{a^2}\sqrt{\left(\frac{D}{\rho h}\right)}. \tag{A8}$$

The modes are given by

$$U_{mn}(r,\theta) = \left[\mathrm{J}_n(\lambda_{mn} r) + \frac{B_2}{B_1}\mathrm{I}_n(\lambda_{mn} r)\right]\cos(n\theta), \tag{A9}$$

where

$$\frac{B_2}{B_1} = -\frac{\mathrm{J}_n(\lambda_{mn} a)[n(n-1) - (\lambda_{mn} a)^2 - \nu n(n-1)] + \mathrm{J}_{n+1}(\lambda_{mn} a)[(\lambda_{mn} a(1-\nu))]}{\mathrm{I}_n(\lambda_{mn} a)[n(n-1) - (\lambda_{mn} a)^2 - \nu n(n-1)] - \mathrm{I}_{n+1}(\lambda_{mn} a)[(\lambda_{mn} a(1-\nu))]} \tag{A10}$$

whilst for a forced response the modal participation factors are obtained from

$$\psi_{mn} = \frac{F_{mn} e^{i\omega t}}{\omega_{mn}^2 - \omega^2 + i\eta\omega_{mn}^2}, \tag{A11}$$

where

$$F_{mn} = \frac{1}{\rho h N_{mn}} \int_0^a \int_0^{2\pi} \left[ q_n(r, \theta) U_{mn}(r, \theta) + \frac{U_{mn}(r, \theta)}{r} \left( \frac{\partial (T(r, \theta) r}{\partial r} \right) \right] r \mathrm{d}\theta \, \mathrm{d}r \tag{A12}$$

and

$$N_{mn} = \int_0^a \int_0^{2\pi} U_{mn}^2(r, \theta) \, r \mathrm{d}\theta \, \mathrm{d}r . \tag{A13}$$

## APPENDIX B: DETAILS OF THE CYLINDER MOBILITIES

Assuming simply supported edges for the cylinder, the following boundary conditions have to be satisfied:

$$U_3(0, \theta) = 0, \tag{B1}$$

$$U_\theta(0, \theta) = 0, \tag{B2}$$

$$M'_{x\theta}(0, \theta) = 0, \tag{B3}$$

$$N'_{xx}(0, \theta) = 0, \tag{B4}$$

$$U_3(L, \theta) = 0, \tag{B5}$$

$$U_\theta(L, \theta) = 0, \tag{B6}$$

$$M'_{x\theta}(L, \theta) = 0, \tag{B7}$$

$$N'_{xx}(L, \theta) = 0. \tag{B8}$$

Accordingly, the eigenfrequencies can be found to be given by

$$\omega_{1mn}^2 = -\frac{2}{3} \sqrt{a_1^2 - 3a_2} \cos\left(\frac{\alpha}{3}\right) - \frac{a_1}{3}, \tag{B9}$$

$$\omega_{2mn}^2 = -\frac{2}{3}\sqrt{a_1^2 - 3a_2}\cos\left(\frac{\alpha + 2\pi}{3}\right) - \frac{a_1}{3}, \tag{B10}$$

$$\omega_{3mn}^2 = -\frac{2}{3}\sqrt{a_1^2 - 3a_2}\cos\left(\frac{\alpha + 4\pi}{3}\right) - \frac{a_1}{3}, \tag{B11}$$

where

$$\alpha = \cos^{-1}\left(\frac{27a_3 + 2a_1^3 - 9a_1a_2}{2\sqrt{(a_1^2 - 3a_2}}\right), \tag{B12}$$

$$a_1 = -\frac{1}{\rho h}(k_{11} + k_{22} + k_{33}), \tag{B13}$$

$$a_2 = \frac{1}{(\rho h)^2}(k_{11}k_{33} + k_{22}k_{33} + k_{11}k_{22} - k_{23}^2 - k_{12}^2 - k_{13}^2), \tag{B14}$$

$$a_3 = \frac{1}{(\rho h)^3}(k_{11}k_{33}^2 + k_{22}k_{13}^2 + k_{33}k_{12}^2 + 2k_{12}k_{23}k_{13} - k_{11}k_{22}k_{33}), \tag{B15}$$

$$k_{11} = K\left[\left(\frac{m\pi}{L}\right)^2 + \frac{1-\mu}{2}\left(\frac{n}{a}\right)^2\right], \tag{B16}$$

$$k_{12} = K\frac{1+\mu}{2}\frac{m\pi}{L}\frac{n}{a}, \tag{B17}$$

$$k_{13} = \frac{\mu K}{a}\frac{m\pi}{L}, \tag{B18}$$

$$k_{22} = \left(K + \frac{D}{a^2}\right)\left[\frac{1-\mu}{2}\left(\frac{m\pi}{2}\right)^2 + \left(\frac{n}{a}\right)^2\right], \tag{B19}$$

$$k_{23} = -\frac{K}{a}\frac{n}{a}\left[\left(\frac{m\pi}{L}\right)^2 + \left(\frac{n}{a}\right)^2\right], \tag{B20}$$

$$k_{33} = D\left[\left(\frac{m\pi}{L}\right)^2 + \left(\frac{n}{a}\right)^2\right]^2 + \frac{K}{a^2} \tag{B21}$$

for which $K$ is the so-called membrane stiffness,

$$K = \frac{Eh}{(1-\mu^2)}. \tag{B22}$$

The fact that for each mode $(m, n)$ there are three frequencies stems from the three displacement components possible in the cylinder, i.e., one flexural and two planar.

From the natural frequency solutions, the corresponding modes of vibration are found to be

$$U_{x,mn}(x, \theta) = \frac{A_i}{C_i} \cos\left(\frac{m\pi x}{L}\right) \cos(n\theta), \tag{B23}$$

$$U_{\theta,mn}(x, \theta) = \frac{B_i}{C_i} \sin\left(\frac{m\pi x}{L}\right) \sin(n\theta), \tag{B24}$$

$$U_3(x, \theta) = C_i \sin\left(\frac{m\pi x}{L}\right) \cos(n\theta), \tag{B25}$$

where

$$\frac{A_i}{C_i} = -\frac{k_{13}(\rho h\omega_{imn}^2 - k_{22}) - k_{12}k_{23}}{(\rho h\omega_{imn}^2 - k_{11})(\rho h\omega_{imn}^2 - k_{22}) - k_{12}^2}, \tag{B26}$$

$$\frac{B_i}{C_i} = -\frac{k_{23}(\rho h\omega_{imn}^2 - k_{11}) - k_{12}k_{13}}{(\rho h\omega_{imn}^2 - k_{11})(\rho h\omega_{imn}^2 - k_{22}) - k_{12}^2}, \tag{B27}$$

$$C_i = 1. \tag{B28}$$

## APPENDIX C: SYMBOLS AND NOTATION

| | |
|---|---|
| $A$ | function |
| $B$ | function |
| $D$ | flexural stiffness |
| $E$ | Young's modulus |
| $F$ | force |
| I | modified Bessel function |
| J | Bessel function |
| K | modified Bessel function |
| $K$ | constant |
| $K$ | membrane stiffness |
| $L$ | length of cylinder |
| $M$ | moment |
| $N$ | force per unit length |
| $Q$ | complex power |
| $T$ | moment |
| $U$ | displacement |
| $W$ | transmitted power |
| $Y$ | mobility |
| $Y$ | Neumann function |
| $a$ | radius |
| $h$ | thickness |

| | |
|---|---|
| i | imaginary unit |
| $r$ | polar co-ordinate |
| $q$ | force |
| $t$ | time |
| $v$ | translational velocity |
| $w$ | rotational velocity |
| $x$ | length |
| $\delta$ | Dirac's delta function |
| $\delta$ | small distance |
| $\eta$ | material loss factor |
| $\lambda$ | eigenfrequency |
| $\nu$ | Poissons' ratio |
| $\theta$ | polar co-ordinate |
| $\rho$ | density |
| $\omega$ | angular frequency |
| $\psi$ | modal participation factor |
| $\sigma$ | stress |
| $\zeta$ | complex variable |

*Indices*

| | |
|---|---|
| $B$ | flexural |
| $L$ | longitudinal |
| $F$ | force |
| $M$ | moment |
| com | "complete" |
| cyl | "cylinder" |
| gui | "guided" |
| $m$ | order |
| $m$ | location |
| $n$ | order |
| $n$ | location |
| red | "reduced" |
| sim | "simplified" |
| $v$ | translational velocity |
| $w$ | rotational velocity |
| 0 | excitation location |

*Notation*

| | |
|---|---|
| . | time differentiation |